# Filtered Lebedev Quadrature Method for Robust and Efficient Beam Shape Coefficients Estimation in Acoustic Tweezers Calibration

Sarah Vincent, R. Marchiano, Jean-Louis Thomas

# Filtered Lebedev Quadrature Method for Robust and Efficient Beam Shape Coefficients Estimation in Acoustic Tweezers Calibration

Sarah Vincent,[1,2] Régis Marchiano,[2] and Jean-Louis Thomas[1,a]

[1]*Sorbonne Université, CNRS, Institut des Nanosciences de Paris, INSP, F-75005 Paris, France*

[2]*Sorbonne Université, CNRS, Institut Jean le Rond d'Alembert, d'Alembert, F-75005 Paris, France*

(Dated: 21 November 2023)

Acoustic tweezers offer a contactless, three-dimensional, and selective approach to trapping objects by harnessing the acoustic radiation force. Precise control of this technique necessitates accurate calibration of the force, which depends on the object's properties and the spherical harmonics expansion of the incident field through the beam shape coefficients. Previous studies showed that these coefficients can be determined using either the Lebedev quadrature or the angular spectrum methods. However, the former is highly susceptible to noise, while the latter demands extensive implementation time due to the number of required measurement points. A filtered method with reduced number of points is introduced to address these limitations. Initially, we emphasize the implicit filtering in the angular spectrum method, allowing relative noise insensitivity. Subsequently, we present its unfiltered version, enabling force estimation of a standing field. Finally, we develop a filtered method based on the Lebedev quadrature, requiring fewer points and apply it to focused vortex beams. Numerical evaluation of the radiation force demonstrates the method's resilience to noise and a reduced need for points compared to previous method. The filtered Lebedev method paves the way for characterizing high-frequency acoustic tweezers, where measurement constraints necessitate rapid and robust beam shape coefficient estimation techniques.

[a]Electronic mail: jean-louis.thomas@sorbonne-universite.fr

## I. INTRODUCTION

Acoustic tweezers recently emerged as a new tool for contactless manipulation of small objects such as cells and molecules. This device is based on radiation force which is the result of the nonlinear interaction of an acoustic field with a solid or fluid obstacle. Many authors[1,2] have tackled the theoretical expression of this force depending on assumptions, one of them stands out by its generality and few assumptions, which are a linear harmonic propagation and a spherical elastic scatterer[3]. This theoretical development results in three-dimensional expressions for the radiation force vector which depend on the beam shape coefficients (BSC) of the incident field and on the scattering coefficients of the spherical object. The BSC correspond to the spherical harmonics expansion of the incident acoustic field and the scattering coefficients depend on the object's size and mechanical properties. Theoretical[3,4] and experimental[5,6] studies proved that three-dimensional trapping can be achieved by emitting a highly focused vortex beam, giving rise to single beam acoustic tweezers. This kind of field possesses a helical singularity which produces a node pressure on the propagation axis and a strong pressure ring around it.

Acoustic tweezers could answer a strong demand in domains such as biophysics as they provide accuracy and accessibility to the sample, compared to standing waves[2]. Many applications can be considered for acoustic tweezers, like the study of biophysical properties of cells and molecules or micro-rheology. For all applications mentioned before, calibration of the radiation force produced by the acoustic tweezers must be conducted. One way of achieving that is to experimentally measure the stiffness of the trap by studying the motions of the trapped object[7–12], provided that the trapping is easily done. Another indirect way of calibrating the tweezers is to measure its incident field using a calibrated sensor and then use a BSC determination method[13,14] to finally compute the radiation force for a known scatterer.

Two kinds of method have been studied, spatially filtered and unfiltered methods. The first type is based on filtering standing waves, which can be produced by experimental noise in a progressive acoustic beam. This insures that the method is not very sensitive to noise. However, the main existing method, the angular spectrum method[13,14] (ASM), requires a very high number of measuring points. The second type is not filtering standing waves, like the Lebedev quadrature method[14] which is based on computing the scalar product of the acoustic field with the spherical harmonics on a small optimized set of points. However, this method is very sensitive to noise. The previous studies indicated that the ASM is the most accurate available method, in the presence of noise, to recover the BSC from incident field measurements, but requires a very large number of points. This can be a problem when using an unstable or sensitive measuring sensor, like an interferometer which allows very fine resolution for the measurement of high-frequency focused vortex beams. An optimal method would combine spatial filtering of standing waves and a reduced number of measurement points. Previous works have shown that spherical measurement arrays enable for the accurate reconstruction of noisy acoustic sound fields[15–17] and are thus the geometry studied here. The present work proposes a BSC determination method featuring these two properties. The paper is organized as follows: Section II recalls the developed theory related to acoustic tweezers. Section III highlights the presence of standing wave filtering in the angular spectrum method. Section IV provides a new optimized filtered method.

## II. THEORETICAL BACKGROUND

### A. Radiation force exerted by an arbitrary incident field on an arbitrarily located spherical elastic scatterer

Radiation pressure results from the variation of a momentum flux due to the presence of an obstacle in the propagation path of a sound field. The analytical expressions of the components of the radiation force exerted on a spherical elastic particle by an arbitrary sound field are defined in the Cartesian coordinate system $(x, y, z)$ by[3,13,18], see also for a review and for a comparison of the different expressions[1,19]:

$$F_x = -\frac{\langle V \rangle}{k_0^2} \sum_{n=0}^{\infty} \sum_{m=-n}^{n} \Im\{Q_n^{-m} A_n^{m*} A_{n+1}^{m-1} C_n + Q_n^m A_n^m A_{n+1}^{m+1*} C_n^*\}, \tag{1}$$

$$F_y = +\frac{\langle V \rangle}{k_0^2} \sum_{n=0}^{\infty} \sum_{m=-n}^{n} \Re\{Q_n^{-m} A_n^{m*} A_{n+1}^{m-1} C_n + Q_n^m A_n^m A_{n+1}^{m+1*} C_n^*\}, \tag{2}$$

$$F_z = -2\frac{\langle V \rangle}{k_0^2} \sum_{n=0}^{\infty} \sum_{m=-n}^{n} \Im\{G_n^m A_n^{m*} A_{n+1}^m C_n\}. \tag{3}$$

With

$$\langle V \rangle = \frac{p_0^2}{4\rho_0 c_0^2},$$

$$C_n = R_n^* R_{n+1} + 2R_n^* R_{n+1},$$

$$Q_n^m = \sqrt{\frac{(n+m+1)(n+m+2)}{(2n+1)(2n+3)}},$$

$$G_n^m = \sqrt{\frac{(n+m+1)(n-m+1)}{(2n+1)(2n+3)}},$$

where $p_0$ is the pressure amplitude of the incident field, $\rho_0$ and $c_0$ are respectively the density and sound velocity of the surrounding medium, $R_n$ are the scattering coefficients depending only on the sphere radius and its mechanical properties. Finally, $A_n^m$ are the beam shape coefficients (BSC) of the incident field $p$, corresponding to the amplitude associated to each spherical wave of degree $n$ and order $m$. These coefficients enable the expansion of the incident field in spherical harmonics such that:

$$p(r,\theta,\varphi) = p_0 \sum_{n=0}^{\infty} \sum_{m=-n}^{n} A_n^m j_n(k_0 r) Y_n^m(\theta,\varphi), \tag{4}$$

with $k_0 = \omega_0/c_0$ the wave number and $(r,\theta,\varphi)$ the spherical coordinates expressed by $x = r\sin\theta\cos\varphi$, $y = r\sin\theta\sin\varphi$, $z = r\cos\theta$. The incident field is assumed to be harmonic such that its omitted time dependence is $e^{-i\omega_0 t}$. The spherical harmonics $Y_n^m$ are defined as:

$$Y_n^m(\theta,\varphi) = \sqrt{\frac{2(n+1)}{4\pi}\frac{(n-m)!}{(n+m)!}} e^{im\varphi} P_n^m(\cos\theta). \tag{5}$$

Computing the radiation force requires knowing the scattering coefficients and the BSC, i.e. knowing the mechanical properties and size of the spherical elastic scatterer, as well as the acoustic incident field.

### B. Acoustic focused vortex beam for three-dimensional trapping

While the method developed here for the BSC reconstruction from measurements is general, it will be illustrated in the context of single beam acoustic tweezers. The main advantages of this type of field for contactless acoustic manipulation are the three-dimensionality, selectivity and accuracy of the trap. Depending on the contrast factor between the object and the medium the trap may require a minimum or a maximum of intensity at the focus. For instance, stiffer and heavier particles are attracted to areas of negative gradient, i.e. to the pressure nodes. Three dimensional trapping has been demonstrated numerically[3,4] and experimentally[5,20] using focused acoustical vortices. The axial force generated by acoustical vortices of order 0[21], 1[22] and higher[23] has been studied previously, see also[24]. The focused acoustic vortex beam can be expanded in spherical harmonics by Eq (4), with[4]:

$$\begin{aligned} A_n^{m,th} =& \delta_{m,m'} 4\pi (k_0 r_0)^2 N_n^{m'} h_n^{(1)}(k_0 r_0) \\ & \times \int_{\pi-\alpha_0}^{\pi} P_n^{m'}(\cos\theta') \sin\theta' \, \mathrm{d}\theta', \end{aligned} \tag{6}$$

$$\delta_{m,m'} = \begin{cases} 1 & \text{if } m = m' \\ 0 & \text{if } m \neq m', \end{cases}$$

the BSC of the incident focused vortex field propagating along the $z$ direction. These coefficients are non-zero only for the order $m = m'$. In this study $m' = 1$, although higher topological charges also allow contactless manipulation[3,6,25]. The parameters $r_0$ and $\alpha_0$ are respectively the focusing distance and the aperture angle.

The BSC of the focused vortex, computed for a 50 MHz frequency in water ($c_0 = 1497$ m/s and $\rho_0 = 997$ kg/m$^3$), a topological charge $m' = 1$, $r_0 = 3$ mm and $\alpha_0 = 50°$, are shown

Fig. 1 (A). The associated pressure field is rendered Fig. 1 (B). Finally, the cylindrical components of the radiation force exerted on a spherical silica bead (of density $\rho_p = 2200$ kg/m$^3$, longitudinal velocity $c_L = 5800$ m/s and transverse velocity $c_T = 3500$ m/s) of radius $0.2\lambda$, with $\lambda = c_0/f_0$ the acoustic wavelength, about 30 $\mu$m, are plotted Fig. 1 (C). The lateral forces, $F_\rho$ and $F_\varphi$ cancel at the origin. The radial force exhibits a negative part away from the centre, tending to attract the bead towards it. The azimuthal force tends to rotate the bead when moved away from the centre. The axial force acts as a restoring force as the parts on either side of the centre are directed towards it, thus establishing a three-dimensional equilibrium position allowing selectivity.

### C. Beam shape coefficients (BSC) determination

The scattering coefficients $C_n$ in Eqs. (1)-(3) can be computed analytically from the values of the mechanical properties and size of the spherical elastic scatterer[3]. The task is then reduced to the computation of the BSC of the incident field. Several methods have been explored[13,14] and fall into two main categories: unfiltered methods and spatially filtered methods.

#### *1. Unfiltered method: Lebedev quadrature*

Using the orthogonality property of the spherical harmonics, the beam shape coefficients can be expressed from the incident pressure field:

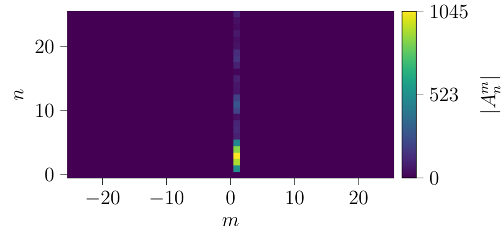


(A) Modulus of the beam shape coefficients.

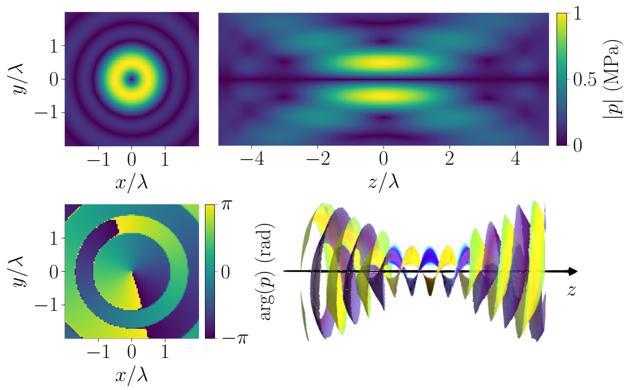


(B) Modulus (top) and phase (bottom) of the pressure field.

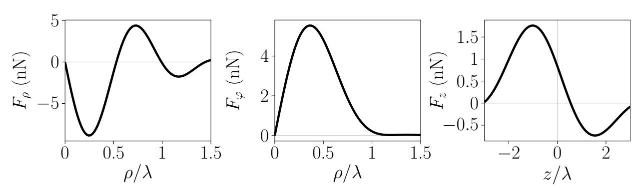


(C) Cylindrical components of the radiation force.

FIG. 1. (Color online) Highly focused acoustic vortex beam propagating along $z$ at a 50 MHz frequency in water. (A) Beam shape coefficients of the focused vortex of topological charge $m' = 1$, focusing distance $r_0 = 3$ mm and aperture angle $\alpha_0 = 50°$. (B) Modulus (top) and phase (bottom) of the pressure field in the transverse (left) and axial (right) planes. The maximum pressure amplitude is set to 1 MPa. (C) Radiation force exerted on a 7 $\mu$m radius silica bead. The lateral components $F_\rho$ and $F_\varphi$ are computed for $z = 0$ and the axial component $F_z$ for $\rho = 0$ in the cylindrical coordinate system.

$$
\begin{aligned}
A_n^m &= \frac{1}{p_0 j_n(k_0 r)} \left\langle p, Y_n^m \right\rangle, \\
&= \frac{1}{p_0 j_n(k_0 r_S)} \int_{\theta=0}^{\pi} \int_{\varphi=0}^{2\pi} p(r_S, \theta_S, \varphi_S) \\
&\qquad \times Y_n^{m*}(\theta_S, \varphi_S) \sin\theta_S \, \mathrm{d}\theta_S \, \mathrm{d}\varphi_S,
\end{aligned}
\tag{7}
$$

with $p(r_S, \theta_S, \varphi_S)$ the incident pressure field measured on a sphere of radius $r_S$.

A way to approximate the surface integral on the sphere is to use the Lebedev quadrature[26]. To compute the force, series are truncated at order $N = 25$. To be consistent, the number of points used in the Lebedev quadrature has to be 975[27]. However, this method is very sensitive to noise. As the scalar product is a linear operation, the complete result is the sum of the scalar product with the theoretical field and the scalar product with the noise. Thus, the method has an error proportional to $1/j_n(k_0 r_S)$, which can be very high for some integrating sphere radii $r_S$. Indeed, the noise is strongly amplified when $j_n$ approaches 0 for some $r_S$. In particular for $j_0(kr_s) = \sin(kr_s)/(kr_s)$ when $r_S/\lambda = l/2$, with $l \in \mathbb{N}^+$. The estimation of the force with this method can therefore work if the radius of the integrating sphere is well chosen, for example $r_S = 5.6\lambda$[14]. On the other hand, if the radius corresponds to the cancellation of $j_n$, e.g. for $r_S = 7\lambda$, then the error explodes for each component of the force.

In the case of such problematic sphere radii, it is possible to reduce the error by cancelling the $A_0^0$ term of the BSC. Then the error remains relatively small and the estimated force approaches its theoretical value. However it has been shown[14] that the axial component shows oscillations. These oscillations have a period close to half a wavelength suggesting the presence of standing waves, presumably produced by the addition of random noise to the acoustic field. Moreover it is known that standing waves tend to produce stronger radiation forces than progressive waves[28]. Thus filtering of the standing waves, in the case of the progressive field, is optimal for the estimation of the radiation force from the determination of the BSC[14].

### *2. Filtered method: Angular spectrum method (ASM)*

A filtered method for the determination of the BSC, applied to a progressive beam, consists in spatially filtering the standing waves components resulting from the presence of noise. The angular spectrum method[13,14] (ASM), based on the plane wave expansion of the incident field and on the Fourier transform, implements an implicit filtering of the standing waves, which will be demonstrated in section III. First a reminder of the ASM[13] is given. If the acoustic field is known in a transverse plane, arbitrarily chosen in $z = 0$, and is an integrable function then the two-dimensional spectrum or angular spectrum is:

$$S_0(k_x, k_y) = \iint\limits_{-\infty}^{\infty} p(x, y, z = 0) e^{-i(k_x x + k_y y)}\, \mathrm{d}x\, \mathrm{d}y. \tag{8}$$

Then the pressure field at any position $z$ is defined by:

$$p(x, y, z) = \frac{1}{(2\pi)^2} \iint\limits_{k_x^2 + k_y^2 \leq k_0^2} S_0(k_x, k_y) e^{i k_z z} e^{i(k_x x + k_y y)}\, \mathrm{d}k_x\, \mathrm{d}k_y, \tag{9}$$

where $k_z = \sqrt{k_0^2 - k_x^2 - k_y^2}$. The integral limit stems from the dispersion relation and results in the filtering of evanescent waves. Then, from the plane wave expansion of the integrand $e^{i\vec{k}\cdot\vec{r}}$ in spherical coordinates:

$$e^{i\vec{k}\cdot\vec{r}} = 4\pi \sum_{n=0}^{\infty} \sum_{m=-n}^{n} i^n j_n(k_0 r) Y_n^m(\theta, \varphi) Y_n^{m*}(\theta_k, \varphi_k), \tag{10}$$

where $\theta_k = \arccos(k_z/k_0)$ and $\varphi_k = \arctan(k_y/k_x)$ and its injection in Eq. (9), the BSC are identified using Eq. (4):

$$A_n^m = \frac{i^n}{\pi} \iint_{k_x^2+k_y^2\leq k^2} S_0(k_x, k_y) Y_n^{m*}(\theta_k, \varphi_k) \, \mathrm{d}k_x \, \mathrm{d}k_y. \tag{11}$$

Note that the pressure amplitude coefficient $p_0$ is now included in the BSC. This method requires knowledge of the sound field on a sufficiently large and fine mesh, otherwise integration errors may occur. In the case of an adequate mesh, the reconstructed BSC are in good agreement with the theoretical ones for $m = m'$ the topological charge of the vortex, but noisy elsewhere. The reconstructed force does not exhibit oscillations, unlike the first unfiltered method[14].

## III. IMPLICIT FILTERING IN THE ASM

We propose to demonstrate that the ASM[13], recalled in section II C 2, is implicitly using a spatial filtering of the standing waves. Then, an unfiltered ASM will be developed.

### A. Application to a standing wavefield

The ASM is applied to a standing field, defined by the following BSC:

$$A_n^{m,stat} = \frac{1}{2}\left[A_n^{m,th} + \left(A_n^{m,th} e^{i\pi}\right)^*\right], \tag{12}$$

where $A_n^{m,th}$ are the theoretical BSC defined by Eq. (6) for the progressive focused vortex, and $A_n^{m,th*}$ their conjugates. Once again, note that the theoretical BSC are including the pressure amplitude coefficients $p_0$, therefore their amplitude is different from the ones shown

Fig. 1 (A). The resulting maximal amplitude of the progressive pressure field is 1 MPa, as well as for the standing pressure field, due to the 1/2 coefficient in Eq. (12).

The BSC $A_n^{m,stat}$ associated with the standing field are shown Fig. 2 (A). The main effect of standing waves features appears along the $m = m' = 1$ axis where the $A_n^{m'}$ are discontinuous compared to the progressive version (cf. Fig 1 (A)). This can be explained by Eq. (4) and the following parity property of the associated Legendre polynomials involved in the spherical harmonics, Eq. (5):

$$P_n^m(-x) = (-1)^{n+m} P_n^m(x) \tag{13}$$

where $x = \cos\theta$, and the angle $\pi - \theta$ corresponds to the direction opposite to that of the progressive field. One coefficient out of every two will therefore cancels and the other will be added, hence the 1/2 factor in Eq. (12). The resulting pressure field, Fig. 2 (B), does show standing waves features along the propagation axis $z$.

In order to demonstrate the implicit filtering of standing waves components, the angular spectrum recalled section II C 2 defined by Eq. (11) is applied to the ”standing focused vortex”, i.e the superposition of two counterpropagating focused vortex, described previously. To do so, the theoretical BSC, Eq. (12), are used to compute the pressure field from Eq. (4) onto a plane at $z = 0$ of dimensions $6\lambda \times 6\lambda$ and 3721 points, corresponding to a spatial sampling of $\lambda/10$. As seen Fig. 2 (B), the resulting maximum pressure amplitude $P_{max}$ of the field is 1 MPa around the focus. To match real experimental conditions, random noise is then added to the pressure field and its maximum amplitude is 5% of $P_{max}$. Finally, Eq. (11) is employed to estimate the BSC, which are plotted Fig. 3. It appears that the ASM does not render the standing wavefield. The obtained BSC are closer to the progressive version

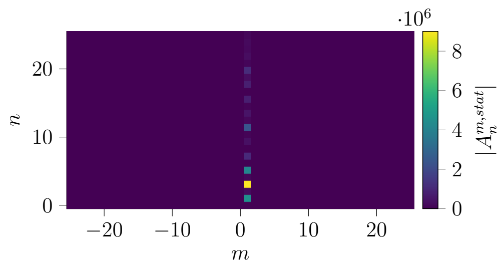


(A) Modulus of the BSC.

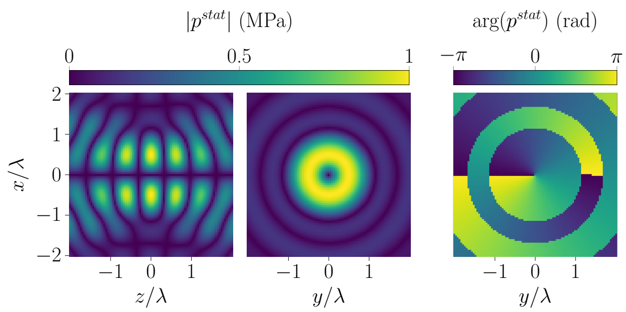


(B) Modulus (left) and phase (right) of the pressure field.

FIG. 2. (Color online) Theoretical BSC and pressure field of the standing focused vortex beam defined by Eq. (12). The pressure field is plotted in the propagation plane $(Oxz)$ and in the transverse plane $(Oxy)$ as well.

of the field (cf. Fig. 1 (A)) indicating an implicit filtering of the standing waves.

### B. Unfiltered ASM

The implicit filtering of standing waves can be removed from the previous ASM. The starting point is the three-dimensional Fourier transform of the harmonic acoustic field:

$$\mathrm{TF}_{3\mathrm{D}}\left[p(\vec{r})\right] = P(\vec{k}) = \int_{\vec{r}\in\mathbb{R}^3} p(\vec{r})e^{-i\vec{k}\cdot\vec{r}}\,\mathrm{d}^3\vec{r}, \tag{14}$$

where $\vec{r} = x\vec{e}_x + y\vec{e}_y + z\vec{e}_z$ is the spatial coordinates vector, and $\vec{k} = k_x\vec{e}_x + k_y\vec{e}_y + k_z\vec{e}_z$ the wave vector. The field being solution of the Helmholtz equation, the dispersion relation $k_x^2 + k_y^2 + k_z^2 = k_0^2$ , with $k_0 = \omega_0/c_0$, imposes

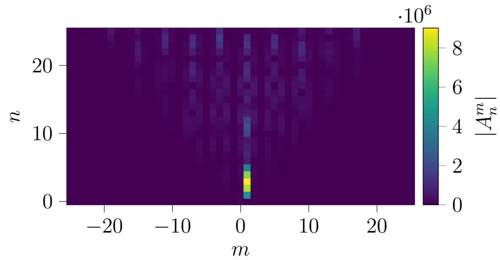


FIG. 3. (Color online) Modulus of the BSC of the standing focused vortex field (cf. Fig 2 (A)) estimated using the filtered ASM, Eq. (11), on the plane located in $z = 0$ of dimensions $6\lambda \times 6\lambda$ sampled in 3721 points.

$$k_z = \pm\sqrt{k_0^2 - k_x^2 - k_y^2} = \pm q. \tag{15}$$

Then, Eq. (14) becomes:

$$\mathrm{TF}_{\mathrm{3D}}\left[p(\vec{r})\right] = P(\vec{k})\left[\delta(k_z - q) + \delta(k_z + q)\right]. \tag{16}$$

The sound field is simply the inverse Fourier transform of $P$ such that:

$$p(\vec{r}) = \frac{1}{(2\pi)^3}\int_{\vec{k}\in\mathbb{R}^3} P(\vec{k})e^{i\vec{k}\cdot\vec{r}}\,\mathrm{d}^3\vec{k}. \tag{17}$$

Using the plane wave expansion Eq. (10) and applying the dispersion relation (cf. Eq. (15)), Eq. (17) becomes:

$$\begin{aligned} p(\vec{r}) = &\sum_{n=0}^{\infty}\frac{i^n}{2\pi^2}j_n(k_0 r)\sum_{m=-n}^{n}Y_n^m(\vec{r}) \\ &\times \iint\limits_{k_x^2+k_y^2\leq k_0^2}\left[P(k_x,k_y,q)Y_n^{m*}(k_x,k_y,q)\right. \\ &\left.+P(k_x,k_y,-q)Y_n^{m*}(k_x,k_y,-q)\right]\mathrm{d}k_x\,\mathrm{d}k_y, \end{aligned}$$

The spherical harmonics can be written as $Y_n^{m*}(\theta_k,\varphi_k)$ with $\cos\theta_k = k_z/k_0$ and $\tan\varphi_k =$

$k_y/k_x$. The associated Legendre polynomials parity Eq. (13) with $x = \cos\theta_k = k_z/k_0 = \pm q/k_0$ yields:

$$p(\vec{r}) = \sum_{n=0}^{\infty} \frac{i^n}{2\pi^2} j_n(k_0 r) \sum_{m=-n}^{n} Y_n^m(\vec{r})$$
$$\times \iint\limits_{k_x^2+k_y^2 \leq k_0^2} \left[P^+ + (-1)^{n+m} P^-\right] Y_n^{m*}(k_x, k_y, q)\, \mathrm{d}k_x\, \mathrm{d}k_y,$$

where $P^+ = P(k_x, k_y, q)$ corresponds to the progressive part of the field and $P^- = P(k_x, k_y, -q)$ to its regressive part. The BSC are identified using the spherical harmonics expansion of the field (cf. Eq. (4)):

$$A_n^m = \frac{i^n}{2\pi^2} \iint\limits_{k_x^2+k_y^2 \leq k_0^2} \left[P^+ + (-1)^{n+m} P^-\right] \times Y_n^{m*}(k_x, k_y, q) dk_x dk_y. \tag{18}$$

Comparing Eq. (8) with Eqs. (14), (15) and (16), the angular spectrum is defined as the inverse Fourier transform of $P(k_x, k_y, k_z)$ with respect to $k_z$:

$$\begin{aligned} S_z(k_x, k_y) &= \frac{1}{2\pi} \int_{-\infty}^{+\infty} P(k_x, k_y, k_z) e^{ik_z z} dk_z, \\ &= \frac{1}{2\pi} \left[P^+ e^{iqz} + P^- e^{-iqz}\right]. \end{aligned}$$

For a progressive wave along the +z-direction, $S_{z=0}(k_x, k_y) = P^+/(2\pi)$, with $S_{z=0}$ the angular spectrum of the acoustic field at plane $z = 0$. From Eq. (18), one thus finds the expression of the BSC given by the filtered ASM[13] (cf. Eq. (11)):

$$A_n^m = \frac{i^n}{\pi} \iint_{k_x^2+k_y^2 \leq k_0^2} S_{z=0}(k_x, k_y) Y_n^{m*}(\theta_k, \varphi_k) dk_x dk_y, \tag{19}$$

For an arbitrary wave, $P^+$ and $P^-$ must be accounted for, it is then necessary to know the angular spectrum on two different planes $z = z_1$ and $z = z_2$:

$$\begin{cases} S_{z_1}(k_x, k_y) = \dfrac{1}{2\pi}\left[P^+ e^{iqz_1} + P^- e^{-iqz_1}\right], \\ \\ S_{z_2}(k_x, k_y) = \dfrac{1}{2\pi}\left[P^+ e^{iqz_2} + P^- e^{-iqz_2}\right]. \end{cases}$$

Leading to:

$$\begin{cases} \left(e^{2iqz_1} - e^{2iqz_2}\right) P^+ = 2\pi\left(S_{z_1} e^{iqz_1} - S_{z_2} e^{iqz_2}\right), \\ \\ \left(e^{-2iqz_1} - e^{-2iqz_2}\right) P^- = 2\pi\left(S_{z_1} e^{-iqz_1} - S_{z_2} e^{-iqz_2}\right). \end{cases} \tag{20}$$

Replacing the pair $(P^+, P^-)$ by $(S_{z_1}, S_{z_2})$ requires avoiding cases where either $\left(e^{2iqz_1} - e^{2iqz_2}\right)$ or $\left(e^{-2iqz_1} - e^{-2iqz_2}\right)$ cancels, see discussion below. By injecting these expressions in Eq. (18):

$$\begin{aligned} A_n^m = \frac{i^n}{\pi} \iint\limits_{k_x^2+k_y^2 \le k_0^2} & \left[\frac{S_{z_1} e^{iqz_1} - S_{z_2} e^{iqz_2}}{e^{2iqz_1} - e^{2iqz_2}}\right. \\ & \left. +(-1)^{n+m} \frac{S_{z_1} e^{-iqz_1} - S_{z_2} e^{-iqz_2}}{e^{-2iqz_1} - e^{-2iqz_2}}\right] Y_n^{m*} dk_x dk_y. \end{aligned} \tag{21}$$

*A priori*, the choice of planes $z_1$ and $z_2$ is arbitrary, here they are chosen symmetrically around the origin, such that $z_1 = -z$ and $z_2 = z$, with $z > 0$, so:

$$\begin{aligned} A_n^m = \frac{i^n}{\pi} & \iint_{k_x^2+k_y^2 \le k_0^2} \frac{1}{2i\sin(2qz)} \\ & \times \left[S_{z^+}\left(e^{iqz} - (-1)^{n+m} e^{-iqz}\right)\right. \\ & \left. - S_{z^-}\left(e^{-iqz} - (-1)^{n+m} e^{iqz}\right)\right] Y_n^{m*} dk_x dk_y. \end{aligned} \tag{22}$$

When $(-1)^{n+m} = 1$:

$$A_n^m = \frac{i^n}{\pi} \iint_{k_x^2+k_y^2 \le k_0^2} \left[\frac{S_{z^+} + S_{z^-}}{2\cos(qz)}\right] Y_n^{m*} dk_x dk_y, \tag{23}$$

and when $(-1)^{n+m} = -1$:

$$A_n^m = \frac{i^n}{\pi} \iint_{k_x^2+k_y^2 \le k_0^2} \left[\frac{S_{z^+} - S_{z^-}}{2i\sin(qz)}\right] Y_n^{m*} dk_x dk_y. \tag{24}$$

As noted above, either $\cos(qz) = 0$ or $\sin(qz) = 0$ may occur. We recognize here special cases like symmetrical and antisymmetrical standing waves with nodes on the chosen planes. To avoid such possibility, a simple solution is to select $0 < qz < \pi/2$, so $0 < z < \lambda/4$ since $q < 2\pi/\lambda$. In the limiting case where $z$ tends toward 0, we recover the case of one single plane at $z = 0$. In this case, Eq. (23) becomes the one obtained in Ref.[13] (see Eq. (11)). While Eq. (24) is new and similar, but $S_z$ is replaced by $(1/iq)\,\mathrm{d}S_z/\,\mathrm{d}z$. Thus the field can be computed everywhere if it is known, as well as its normal derivative, on a plane.

Unlike the filtered method, this complete ASM should be able to estimate the BSC of a standing wavefield like the one defined by Eq. (12). To do so, the theoretical field is computed on two planes taken in $z = -0.1\lambda$ and $z = 0.1\lambda$, their dimensions are $6\lambda \times 6\lambda$ and the number of points is 3721. As before, random noise is numerically added to the pressure field at 5% of its maximum amplitude. The BSC are then estimated using Eq. (22). The reconstructed radiation force is plotted Fig. 4 and compared to the theoretical one and the one obtained from the filtered ASM.

The errors made by each method on the force estimation are defined as:

$$\epsilon(F_\gamma, x) = \frac{100}{N_x} \sum_{j=0}^{N_x-1} \frac{|F_\gamma(x_j) - F_\gamma^{th}(x_j)|}{max|F_\gamma^{th}|} \quad (\%), \tag{25}$$

with $\{F_\gamma, x\} = \{F_\rho, \rho\}, \{F_\varphi, \rho\}, \{F_z, z\}$. As planned, only the unfiltered method recovers the proper force. Furthermore, at equivalent pressure amplitude between the standing and progressive fields, the axial force of the standing wave is twice as large, with respect to the positive peak, and six times larger, with regard to the negative peak. The standing waves therefore have a substantial contribution to the radiation force[28]. The amplitude distribution between the positive and negative peaks of the axial force is balanced. Although slightly overestimated by the filtered methods, the radial force is hardly modified compared to the progressive vortex (cf. Fig 1 (C)). Indeed, the latter already has a standing wave behavior due to the focusing of the field. This amplitude ratio will also depends on the focusing sharpness or aperture angle $\alpha_0$. The azimuthal component, on the other hand, maintains a progressive behavior.

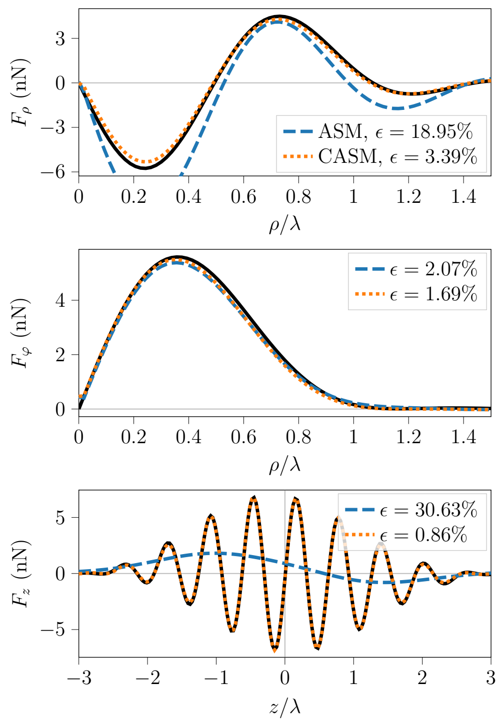


FIG. 4. (Color online) Estimation of the cylindrical components of the radiation force exerted on a 7 $\mu$m silica bead by a standing focused vortex beam (defined by Eq. (12)) using the filtered ASM (Eq (11)) and the unfiltered complete ASM (noted CASM) (Eq.(22)) on a plane located in $z = 0$ for the ASM, and on 2 planes located in $z = \pm 0.1\lambda$ for the CASM. Each plane has dimensions $6\lambda \times 6\lambda$ and is sampled in 3721 points. The theoretical force is plotted in black. The errors $\epsilon$ made by each method on the force are given by Eq. (25).

# IV. NEW BSC DETERMINATION METHOD : FILTERED LEBEDEV METHOD

The existing methods described in section II C are either very sensitive to noise, or very costly in terms of measurement duration, due to the large number of points required to compute the BSC. These two aspects can be particularly problematic when the measurement is noisy or subject to deterioration over the duration of the measurement.
The Lebedev method described in section II C 1 seemed promising given the reduced number of measurement points and their distance from the focal spot, where the dynamics of the measured signals are important. However, it is too sensitive to noise. An improvement of this method would be to add filtering. Indeed, the presence of noise in the acoustic field acts like the presence of a standing wave and filtering this standing wave would reduce the impact of noise on a progressive field. The ASM, which already uses this type of filtering (cf. section III A), is much more robust to noise than the unfiltered Lebedev method. The theoretical development for applying standing wave filtering is described below.

## A. Theoretical development

The starting point of this filtered Lebedev method is to consider a harmonic acoustic field propagating linearly in a homogeneous perfect fluid without any source. Thus, the acoustic field $\Psi(\vec{r})$ verifies the homogeneous Helmholtz equation:

$$(\Delta + k^2)\Psi(\vec{r}) = 0, \tag{26}$$

where $\Psi(\vec{r})$ is the spatial dependence of the field and $e^{-i\omega_0 t}$ its implicit time dependence. This equation can be solved using the Green function $G(\vec{r}|\vec{r_S}) = G$, solution of:

$$(\Delta + k^2)G = -\delta(\vec{r} - \vec{r}_S). \tag{27}$$

The acoustic field is then written[29]:

$$\Psi(\vec{r}) = \iint_S \left[G\nabla\Psi(\vec{r}_S)\cdot\vec{n} - \Psi(\vec{r}_S)\nabla G\cdot\vec{n}\right]\mathrm{d}S. \tag{28}$$

It is determined in the volume contained by $S$, an arbitrary closed surface with outward unit normal $\vec{n}$. In order to have a unique solution, a boundary conditions on $S$ is required, for instance Dirichlet, $\Psi$ is fixed on $S$ or Neumann conditions where $\nabla\Psi\cdot\vec{n}$ is given instead. The homogeneous version of this condition should be used to determine the Green function, $G$. In Kirchhoff approach both $\Psi$ and $\nabla\Psi\cdot\vec{n}$ are fixed on $S$ and the Green function is the Green function of free space, $G_0$ Eq. (29).

$$G = G_0 = \frac{e^{ik_0 R}}{4\pi R}, \text{ where } R = |\vec{r} - \vec{r}_S|. \tag{29}$$

In the following, to simplify the presentation, the closed surface $S$ is chosen as a fictitious spherical surface of radius $r_S$. Thus $\nabla(.)\cdot\vec{n} = \partial(.)/\partial r$. The spherical harmonics expansion of the free space Green function $G_0$, for $r_S > r$ is given by[30]:

$$G_0 = ik_0 \sum_{n,m} j_n(k_0 r) h_n^{(1)}(k_0 r_S) Y_n^{m*}(\theta_S, \varphi_S) Y_n^m(\theta, \varphi), \tag{30}$$

where $(r_S, \theta_S, \varphi_S)$ are the spherical coordinates describing $S$ and $\sum_{n,m} = \sum_{n=0}^{\infty}\sum_{m=-n}^{n}$. Thus,

$$\begin{aligned}\left.\frac{\partial G_0}{\partial r'}\right|_{r'=r_S} = ik_0 \sum_{n,m} j_n(k_0 r) &\left.\frac{\partial h_n^{(1)}(k_0 r')}{\partial r'}\right|_{r'=r_S} \\ &\times Y_n^{m*}(\theta_S, \varphi_S) Y_n^m(\theta, \varphi).\end{aligned} \tag{31}$$

Injecting these last equations in Eq. (28), it becomes:

$$\Psi(r,\theta,\varphi) = -ik_0 \sum_{n,m} j_n(k_0 r) Y_n^m(\theta,\varphi)$$
$$\times \int_0^{2\pi}\int_0^{\pi} \left[ \Psi_S \frac{\partial h_n^{(1)}}{\partial r'}\bigg|_{r'=r_S} - h_n^{(1)}(k_0 r_S) \frac{\partial \Psi}{\partial r'}\bigg|_{r'=r_S} \right] \tag{32}$$
$$\times Y_n^{m*}(\theta_S,\varphi_S) r_S^2 \,\mathrm{d}\Omega,$$

where $\Psi_S = \Psi(r_S,\theta_S,\varphi_S)$ and $\mathrm{d}\Omega = \sin\theta_S \,\mathrm{d}\theta_S \,\mathrm{d}\varphi_S$. Comparing with Eq. (4) to the difference that the amplitude coefficient $\psi_0$ (or $p_0$ in pressure) is included in the BSC yields :

$$A_n^m = -ik_0 r_S^2 \left\langle \Psi \frac{\partial h_n^{(1)}}{\partial r'}\bigg|_{r'=r_S} - h_n^{(1)} \frac{\partial \Psi}{\partial r'}\bigg|_{r'=r_S}, Y_n^m \right\rangle. \tag{33}$$

To facilitate the comparison, we use the notation $\langle \cdot,\cdot \rangle$ of Eq. (7) in place of the integral. We can check its consistency using the expansion of $\Psi(\vec{r})$ in spherical harmonics with another set of BSC:

$$\Psi(r,\theta,\varphi) = \sum_{n,m} B_n^m j_n(k_0 r) Y_n^m(\theta,\varphi), \tag{34}$$

From this expansion, the field on the surface $S$ and its derivative are obtained and injected in Eq. (33). Permuting series and integrals signs and using the orthogonality of the $Y_n^m$, yields:

$$A_n^m = -i\mathrm{x}^2 B_n^m \left[ j_n(\mathrm{x}) \frac{\mathrm{d}h_n^{(1)}(\mathrm{x})}{\mathrm{dx}} - \frac{\mathrm{d}j_n(\mathrm{x})}{\mathrm{dx}} h_n^{(1)}(\mathrm{x}) \right] \tag{35}$$

where $\mathrm{x} = k_0 r_S$. Using the definition $h_n^{(1)}(\mathrm{x}) = j_n(\mathrm{x}) + iy_n(\mathrm{x})$, the bracket of Eq. (35) can be rewritten as $i\,[j_n(\mathrm{x})y_n'(\mathrm{x}) - j_n'(\mathrm{x})y_n(\mathrm{x})]$ where prime stands for derivative. We recognize a Wronskian whose value is $(1/\mathrm{x}^2)$[31] (Chap. 10, Eq. (10.1.6)). We can then confirm the consistency of Eq. (35) since we obtain, as expected from the uniqueness of the solution: $A_n^m = B_n^m$. Note that we chose to replace $h_n^{(1)}(\mathrm{x})$ and its derivative in the bracket. Another equivalent choice is to replace $j_n$ and its derivative using $2j_n(\mathrm{x}) = h_n^{(1)}(\mathrm{x}) + h_n^{(2)}(\mathrm{x})$. In this last case the bracket becomes $(1/2)\left[h_n^{(2)}(\mathrm{x})h_n^{'(1)}(\mathrm{x}) - h_n^{'(2)}(\mathrm{x})h_n^{(1)}(\mathrm{x})\right]$. This shows that even if $\Psi$, as written in Eq. (34), involves $j_n$ and hence the sum of the two Hankel functions, only the incoming part, $h_n^{(2)}$, makes a contribution to the value of the $A_n^m$ while the other part involving $h_n^{(1)}$ cancels out.

Eq. (33) requires the knowledge of both the field and its radial derivative on a closed surface. First, this is not always possible to measure the field and its derivative. Second, assigning a value to both is unnecessary since they are related, see for a review[32]. For single-beam acoustic tweezers the field is progressive and hence enters the surface on the upstream side and leaves on the downstream side, as shown in Fig. 5. For a surface sufficiently far

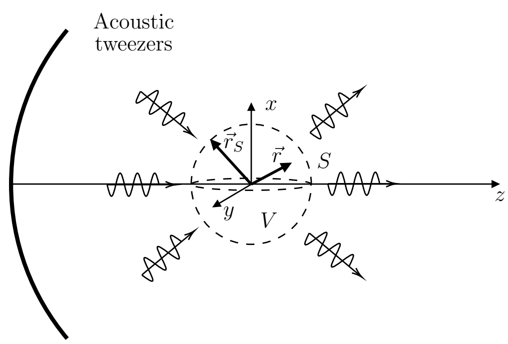


FIG. 5. Configuration of the filtered Lebedev method: if the field is progressive, it is entering the volume where $\theta \in [\pi/2, \pi]$ and outgoing when $\theta \in [0, \pi/2]$, where $\theta = \arccos(r/z)$.

from the area of interest, $k_0 r_S >> 1$, these boundary conditions are enforced by Sommerfeld radiation conditions[33]. With the convention chosen here $\exp(-i\omega t)$, if $\theta_S \in [0, \frac{\pi}{2}]$, i.e downstream:

$$\frac{\partial \Psi_S}{\partial r'}\bigg|_{r'=r_S} \approx (+ik_0 - \tfrac{1}{r_S})\Psi_S \tag{36}$$

while for upstream, $\theta_S \in [\frac{\pi}{2}, \pi]$

$$\left.\frac{\partial \Psi_S}{\partial r'}\right|_{r'=r_S} \approx (-ik_0 - \tfrac{1}{r_S})\Psi_S \tag{37}$$

This last condition, Eq. (36) for outgoing wave, is satisfied by $h_n^{(1)}$ on the whole surface, with $h_n^{(1)}(\mathrm{x}) \approx i^{-n-1}\exp(i\mathrm{x})/\mathrm{x}$[31]. This approximation holds for $k_0 r_S \geq 2N$, especially for the phase of the Hankel functions. Corollary, $h_n^{(2)}$ satisfy Eq. (37) for incoming wave. Using these boundary conditions, Eqs. (36),(37) for the field $\Psi$ and the derivative of the Hankel function, Eq. (33) can be rewritten:

$$\begin{aligned} A_n^m = -ik_0 r_S^2 \int\limits_0^{2\pi} \Bigg\{ \int\limits_{\frac{\pi}{2}}^{\pi} \Big[&(ik_0 - \tfrac{1}{r_S}) h_n^{(1)}(k_0 r_S)\Psi_S \\ -h_n^{(1)}(k_0 r_S)(-ik_0 - \tfrac{1}{r_S})\Psi_S\Big]&\, Y_n^{m*}(\theta_S, \varphi_S)\, \mathrm{d}\Omega \\ &+ \int_0^{\frac{\pi}{2}} \Big[(ik_0 - \tfrac{1}{r_S}) h_n^{(1)}(k_0 r_S)\Psi_S \\ -h_n^{(1)}(k_0 r_S)(ik_0 - \tfrac{1}{r_S})\Psi_S\Big]&\, Y_n^{m*}(\theta_S, \varphi_S)\, \mathrm{d}\Omega \Bigg\}, \end{aligned}$$

In the second integral, the sum of the two terms cancels out so that finally:

$$A_n^m = 2k_0^2 r_S^2 h_n^{(1)}(k_0 r_S) \int_0^{2\pi} \int_{\frac{\pi}{2}}^{\pi} \Psi_S Y_n^{m*}(\theta_S, \varphi_S)\, \mathrm{d}\Omega \tag{38}$$

Eq. (38) requires knowing the field on half the surface, the upstream side. This last feature comes from the noted fact that only the $h_n^{(2)}$ part of $j_n$ contributes to Eq. (35), combined with the boundary conditions Eqs. (36),(37), imposing an incoming field on a single side. Thus by enforcing these conditions, even if the measured field is noisy, the noise can only add random fluctuations on the upstream side. Without the incoming contribution from the downstream side, the noise standing wave content is filtered out.

It is advantageous compared to the ASM because it uses the optimized set of points on the sphere, given by the Lebedev quadrature, and it is sufficient to measure the acoustic field on the fictitious half-sphere between $\theta_S = \pi/2$ and $\theta_S = \pi$, which considerably reduces the number of measurement points (between 229 and 1041, depending on the precision chosen to solve the integral). Moreover, the method directly uses the measured field and not its spatial Fourier transform. Compared to the previous unfiltered method using the Lebedev quadrature, the factor $1/j_n(k_0 r_S)$ (cf. Eq. (7)) generating an important error in the presence of noise does not appear in Eq. (38). Finally, this new filtered Lebedev method allows for the reconstruction of focused acoustic fields at the focal point by measuring them far from areas with strong amplitude dynamics, which is of interest for some dynamic-limited sensors. It is, however, restricted to progressive, harmonic fields propagating in free space, and requires the radius of the spherical surface to be large enough for the spherical Hankel functions and acoustic field approximations to hold.

### B. Numerical validation

The filtered Lebedev method is applied to estimate the BSC of a focused vortex field described by Eq. (6), of frequency $f_0 = 50$ MHz, topological charge $m' = 1$, aperture angle $\alpha_0 = 50°$ and focal distance $r_0 = 3$ mm propagating in water. The validation procedure consists in computing the acoustic field on the spherical surface of integration from the theoretical BSC truncated at $N = 50$. As before, random noise at 5% of the maximum amplitude of the field computed on the half-spherical surface is numerically added. Then, Eq. (38) is solved using a Lebedev quadrature. Thus, the estimated BSC are compared to the theoretical ones, then used to compute the radiation force which is also compared to the theoretical one. This validation process allows determining the optimum numerical parameters, which are the integration sphere radius $r_S$ and the Lebedev quadrature order. In a first step, the quadrature order is studied, the surface radius is set to $10\lambda$, implying a truncation of $N = 30$. The reconstruction of the BSC as well as the calculation of the radiation force is performed for several orders of quadrature listed in the Table I, with the corresponding numbers of measurement points. The Lebedev quadrature is implemented numerically using the Python library *quadpy*.

| Quadrature order | 35 | 41 | 47 | 53 | 59 | 65 | 71 | 77 |
|---|---|---|---|---|---|---|---|---|
| Number of points | 229 | 309 | 401 | 505 | 621 | 749 | 889 | 1041 |

TABLE I. Orders of the Lebedev quadrature and associated numbers of points on the half-sphere defined by $\theta \geq \pi/2$.

The relative error on the estimation of the BSC is given by:

$$\epsilon(A_n^m) = \frac{100}{(N+1)(2N+1)} \sum_{n=0}^{N} \sum_{m=-n}^{n} \frac{|A_n^m - A_n^{m,th}|}{max|A_n^{m,th}|} \quad (\%), \tag{39}$$

and by Eq. (25) for the force cylindrical component. The errors evolving with the order of the quadrature are plotted Fig. 6 (A). The BSC error is much weaker than those related to the radiation force and is stabilizing around 0.15% from a quadrature order of 59. On the other hand, the errors related to the cylindrical components of the force are not monotonic and do not seem to have any specific relationship with the BSC error. The axial component is of particular importance here because, in the case of the vortex, it has the smallest amplitude compared to the others, about one order of magnitude less for the negative peak. However, the axial force is essential to obtain a three-dimensional trap, so interest will be focused on the error made on this component. In addition, we wish to minimise the number of points for the field in order to reduce the measurement duration. A compromise must therefore be made between the error and the number of points. The estimation error related to the axial force is minimal, about 1%, for an order of quadrature of 65 and 71, which corresponds to 749 and 889 points respectively (cf. Table I).

It is now appropriate to study the second parameter of interest, the radius $r_S$ of the half-sphere of integration. This radius must be taken sufficiently large compared to the wavelength so that the asymptotic forms of the spherical Hankel functions hold. This condition numerically imposes $N < \pi r_S/\lambda$. Thus, the radius is varied between $\lambda$ and $10\lambda$, and $N$ according to $r_S$ (cf. Table II). Again, the error on the BSC, Fig. 6 (B), remains very small

| $r_S$ | $1\lambda$ | $2\lambda$ | $3\lambda$ | $4\lambda$ | $5\lambda$ | $6\lambda$ | $7\lambda$ | $8\lambda$ | $9\lambda$ | $10\lambda$ |
|---|---|---|---|---|---|---|---|---|---|---|
| $N$ | 3 | 6 | 9 | 12 | 15 | 18 | 21 | 25 | 28 | 30 |

TABLE II. Radii $r_S$ of the half-sphere of integration and associated truncation orders $N$ of the BSC series.

compared to those on the force and it stabilizes below 0.2% from a radius of $5\lambda$. The errors on the force components seem to oscillate and reach local minimum values at odd radii. The global minimum error on $F_z$ corresponds to a radius of $7\lambda$. The high errors occurring for radii below $5\lambda$ can be caused by an under sizing of the integration sphere and/or a too low truncation order.

The parameters finally retained (cf. Table III) are therefore a half-sphere of radius $r_S = 7\lambda$, allowing a truncation of the BSC series at $N = 21$, a minimum order of quadrature of 65 and therefore 749 measurement points.

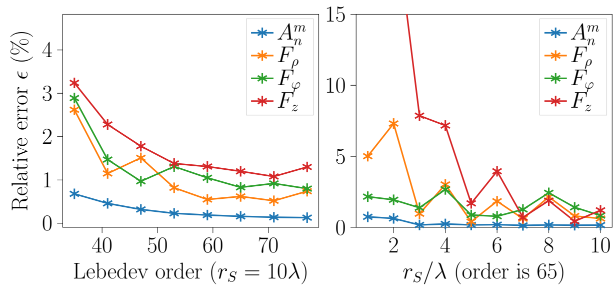


FIG. 6. (Color online) Relative errors of estimation of the filtered method based on the Lebedev quadrature, defined by Eq. (38). The errors for the BSC are computed from Eq. (39) and those for cylindrical components of the radiation force from Eq. (25). On the left the error is expressed in terms of the quadrature order of integration (cf. Table I) while the radius of the integration surface is set to $10\lambda$ (implying a truncation order of the BSC series of $N = 30$). On the right, the error is expressed in terms of the radius of the integration surface (cf. Table II) while the quadrature order is set to 65.

### C. Comparison with previous methods

The new filtered method can be compared to the unfiltered Lebedev method (cf. section II C 1) and to the filtered ASM (cf. section II C 2). The radius of the integration surface

| | |
|---|---|
| Radius $r_S$ | $7\lambda$ |
| Truncation order $N$ | 21 |
| Lebedev quadrature order | 65 |
| Number of points | 749 |

TABLE III. Optimal parameters for the new Lebedev filtered method defined by Eq. (38).

is set to $5.6\lambda$[14] for the unfiltered Lebedev method. The truncation order $N$ and the Lebedev quadrature order are identical to the new filtered method (cf. Table III). The filtered ASM is used on an acoustic field defined in the focal plane (located in $z = 0$) of dimensions $6\lambda \times 6\lambda$ sampled in $61^2 = 3721$ measurement points, corresponding to a sampling step of $\lambda/10$.

The estimated forces by the three different methods are plotted in Fig. IV C. They all properly recover the theoretical force, even though the error is slightly higher for the ASM. It can be reduced by increasing the size and number of points of the measurement plane. The axial force estimated by the unfiltered Lebedev method shows slight oscillations. These oscillations depend on the signal to noise ratio and the radius chosen for the quadrature. The noise acts partly as a standing wave, known to generate much stronger forces than a travelling wave[28]. However, in the absence of filtering, the noise causes oscillations of the axial force, axis on which the focused vortex is progressive. On the contrary, radially $j_n(kr)$ is the sum of two converging and diverging Hankel functions and can be considered as a standing field.

The new filtered Lebedev method therefore provides a low-cost, reliable, noise-insensitive

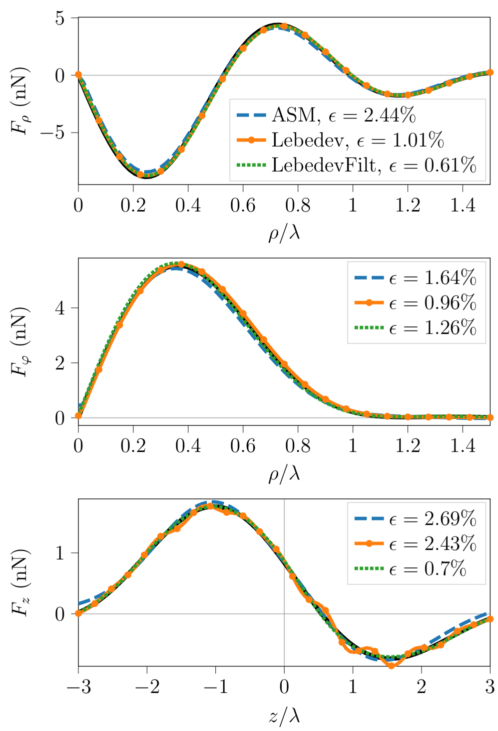


FIG. 7. (Color online) Comparison of the cylindrical components of the radiation force exerted on a 7 $\mu$m silica bead by a progressive focused vortex beam using the filtered ASM (with $z = 0$, and plane dimensions of $6\lambda \times 6\lambda$ sampled in 3721 points) (cf. Eq. (11)), the unfiltered Lebedev method (noted Lebedev, with parameters: $r_S = 5.6\lambda$ and a quadrature order of 65) (cf. Eq. (7)) and the filtered Lebedev method (noted LebedevFilt, with parameters listed in Table. III) (cf. Eq. (38)). The estimations are done with noise of amplitude up to 5% of the maximum pressure field computed on the surface of interest. Each estimated BSC series is truncated at $N = 21$. The theoretical force is plotted in black. The errors $\epsilon$ made by each method on the force are given by Eq. (25).

estimation of the BSC of the acoustic field that allows reconstruction of the radiation force with errors around 1% and lower than 1% for the axial component, while requiring a minimal number of points compared to other methods. The advantages of this method are a spatial filtering of the standing waves which strongly reduces the influence of noise, a limited number of measurement points, chosen specifically for the numerical computation of the integral (cf. Eq. (38)), and the direct use of the measured field instead of its Fourier transform. Moreover, the absence of the $1/j_n$ term, which appears in the first unfiltered Lebedev method, also makes it much more stable.

Finally, the new method is applied to the acoustic tweezers described in previous works on

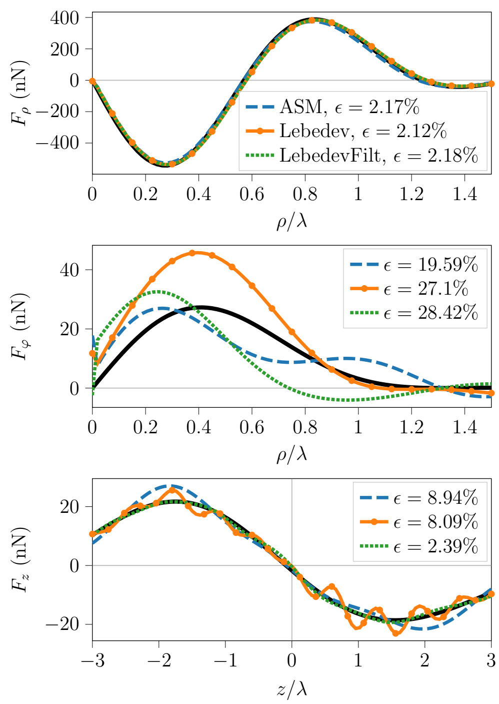


FIG. 8. (Color online) Comparison of the cylindrical components of the radiation force exerted on a $0.1\lambda$ polystyrene bead by a progressive focused vortex beam at frequency 1.2 MHz, aperture angle $\alpha_0 = 43°$, focusing distance $r_0 = 75$ mm, topological charge $m' = 1$ and maximal amplitude 0.8 MPa[14].

beam shape coefficients, see Ref.[14]. The vortex field parameters are $f_0 = 1.2$ MHz, $\alpha_0 = 43°$, $r_0 = 75$ mm, $m' = 1$ and its maximum amplitude is set to 0.8 MPa at the focal plane. As before, the filtered ASM, the unfiltered and filtered Lebedev methods are used to recover the BSC and compute the radiation force exerted on a polystyrene bead of radius $0.1\lambda$ (with $\lambda \approx 1.2$ mm in this case), density $\rho_p = 1080$ kg/m$^3$, longitudinal velocity $c_L = 2350$ m/s and transverse velocity $c_T = 1120$ m/s. Same numerical parameters as before are used for the ASM and unfiltered Lebedev method, but for the filtered Lebedev method, the radius of the integration surface $r_S$ is set to $10\lambda$, resulting in a truncation order $N$ of 25, while the quadrature order of integration is kept as before to 65. Noise is also added as before, to an amount of 5% of the maximum pressure amplitude.

Fig. 8 shows the radiation force recovered by the three previous methods and can be compared to Fig. 7 (left) of Ref.[14]. First, it is noticed that the radial component is equivalently recovered by all methods, with a 2% error. On the other hand, the azimuthal component is not recovered by any method. This component is progressive, defined by $e^{im'\varphi}$, and none of the methods described here are performing azimuthal filtering. Thus, they are all disturbed by noise for this component. Also, the high-frequency acoustic tweezers defined in the present work has an aperture angle of 50°, against 43° for the one defined in Ref.[14]. This results in stronger focusing for the 50 MHz tweezers and in better performance of the BSC determination methods, due to the reduced ratio between the progressive (along $\varphi$ and $z$) and the standing (along $\rho$) waves. Note that the radial to azimuthal forces ratio is about 20 in Ref.[14] and is lower than 2 in the present work. Finally, we recall that the azimuthal force determination can be significantly improved by cancelling the BSC when $m \neq m'$, see the right of Fig. 7 in Ref.[14].

Regarding the axial component of the force, it is best recovered by the new filtered Lebedev method, with an error lower than 3%. Both ASM and the unfiltered Lebedev method show an error of around 9% on $F_z$. As noted before, the ASM does not display oscillations, contrary to the Lebedev method. Moreover, these oscillations are enhanced by the diminution of the aperture angle inducing the increase of stationary effects. The radial to axial forces ratio is about 20 for $\alpha_0 = 43°$ and about 5 for $\alpha_0 = 50°$. In conclusion, the new filtered method is more efficient while requiring fewer measurement points. The filtering is all the more necessary as the beam is weakly focused.

## V. CONCLUSION

Determination of the radiation force is an important process for the calibration of acoustic tweezers. A way to achieve this is to use a BSC determination method applied to a field measurement and then compute the associated force from the BSC $A_n^m$. Two kinds of methods have been previously described, unfiltered, e.g. the Lebedev method, and filtered methods, e.g. the ASM. The first method was proven to be very sensitive to noise, unlike the ASM, due to noise producing standing waves-like behavior. We showed that the good results obtained by the ASM are related to an implicit filtering of the standing waves. Indeed, this filtered method is failing to reconstruct the radiation force produced by a standing focused vortex beam. We presented a complete unfiltered ASM relevant for standing waves and capable of estimating the forces with an error smaller than 2% for the axial component, whereas the filtered ASM is failing. Nevertheless, spatial filtering is essential for the determination of the BSC of progressive fields. Although the filtered ASM is quite efficient, it is experimentally time-consuming owing to the large number of measurement points of the acoustic field. This may be critical. Indeed for high-frequency ultrasound focused field, the spatial features are of the order of the wavelength, about ten micrometers. Scanning such field with a spatial resolution of a few microns is possible with optical interferometers and a high numerical aperture objective to focus the probe arm. However the contrast of the interferometer is now very sensitive to any change of the focus. Therefore, the scan should be finished before the drift in time is significant. Thus, we introduced a new filtered BSC determination method inspired by the Lebedev method. It allows a very accurate reconstruction of the radiation force, with errors smaller than 1%, at a low cost in terms of number of measurement points (half of what is required by the unfiltered Lebedev method). It is insensitive to noise and does not require the use of Fourier transforms. This can avoid some errors related to windowing and spatial sampling of the field. Scanning on a sphere centered at the focus of a sharply focused beam reduces the required dynamic range of the measurement sensor. Furthermore, it removes an additional step of numerical data manipulation. The optimal parameters of this method are studied numerically. Experimental demonstration for focused fields at 50 MHz, wavelength 30 $\mu$m and scanning with an optical interferometer is underway. The experimental set-up and results will be reported in a subsequent paper.

## AUTHOR DECLARATIONS

All authors declare they have no conflict of interest.

## DATA AVAILABILITY

The data that support the findings of this study are available from the corresponding author.

## REFERENCES

[1]M. Baudoin and J.-L. Thomas, "Acoustic Tweezers for Particle and Fluid Micromanipulation," Annual Review of Fluid Mechanics **52**(1), 205–234 (2020) doi: 10.1146/annurev-fluid-010719-060154.

[2]M. A. B. Andrade, N. Pérez, and J. C. Adamowski, "Review of Progress in Acoustic Levitation," Brazilian Journal of Physics **48**(2), 190–213 (2018) doi: 10.1007/s13538-017-0552-6.

[3]D. Baresch, J.-L. Thomas, and R. Marchiano, "Three-dimensional acoustic radiation force on an arbitrarily located elastic sphere," The Journal of the Acoustical Society of America **133**(1), 25–36 (2013) doi: 10.1121/1.4770256.

[4]D. Baresch, J.-L. Thomas, and R. Marchiano, "Spherical vortex beams of high radial degree for enhanced single-beam tweezers," Journal of Applied Physics **113**(18), 184901 (2013) doi: 10.1063/1.4803078.

[5]D. Baresch, J.-L. Thomas, and R. Marchiano, "Observation of a Single-Beam Gradient Force Acoustical Trap for Elastic Particles: Acoustical Tweezers," Physical Review Letters **116**(2), 024301 (2016) doi: 10.1103/PhysRevLett.116.024301.

[6]A. Marzo, M. Caleap, and B. W. Drinkwater, "Acoustic Virtual Vortices with Tunable Orbital Angular Momentum for Trapping of Mie Particles," Physical Review Letters 6 (2018).

[7]S. Vincent, P. Challande, and R. Marchiano, "Calibration of the axial stiffness of a single-beam acoustic tweezers," Review of Scientific Instruments **94**(9), 095102 (2023) doi: 10.

1063/5.0150610.

[8]D. Baresch and V. Garbin, "Acoustic trapping of microbubbles in complex environments and controlled payload release," Proceedings of the National Academy of Sciences **117**(27), 15490–15496 (2020) doi: 10.1073/pnas.2003569117.

[9]A. V. Nikolaeva, S. A. Tsysar, and O. A. Sapozhnikov, "Measuring the radiation force of megahertz ultrasound acting on a solid spherical scatterer," Acoustical Physics **62**(1), 38–45 (2016) doi: 10.1134/S1063771016010048.

[10]M. A. Ghanem, A. D. Maxwell, O. A. Sapozhnikov, V. A. Khokhlova, and M. R. Bailey, "Quantification of Acoustic Radiation Forces on Solid Objects in Fluid," Physical Review Applied **12**(4), 044076 (2019) doi: 10.1103/PhysRevApplied.12.044076.

[11]J. Lee, J. S. Jeong, and K. K. Shung, "Microfluidic acoustic trapping force and stiffness measurement using viscous drag effect," Ultrasonics **53**(1), 249–254 (2013) doi: 10.1016/j.ultras.2012.06.008.

[12]Y. Li, C. Lee, K. Ho Lam, and K. Kirk Shung, "A simple method for evaluating the trapping performance of acoustic tweezers," Applied Physics Letters **102**(8), 084102 (2013) doi: 10.1063/1.4793654.

[13]O. A. Sapozhnikov and M. R. Bailey, "Radiation force of an arbitrary acoustic beam on an elastic sphere in a fluid," The Journal of the Acoustical Society of America **133**(2), 661–676 (2013) doi: 10.1121/1.4773924.

[14]D. Zhao, J.-L. Thomas, and R. Marchiano, "Computation of the radiation force exerted by the acoustic tweezers using pressure field measurements," The Journal of the Acoustical

Society of America **146**(3), 1650–1660 (2019) doi: 10.1121/1.5126095.

[15]B. Rafaely, "The Spherical-Shell Microphone Array," IEEE Transactions on Audio, Speech, and Language Processing **16**(4), 740–747 (2008) doi: 10.1109/TASL.2008.920059.

[16]A. Fahim, P. N. Samarasinghe, and T. D. Abhayapala, "Sound field separation in a mixed acoustic environment using a sparse array of higher order spherical microphones," in *2017 Hands-free Speech Communications and Microphone Arrays (HSCMA)*, IEEE, San Francisco, CA, USA (2017), pp. 151–155, doi: 10.1109/HSCMA.2017.7895580.

[17]D. L. Alon and B. Rafaely, "Spherical microphone array with optimal aliasing cancellation," in *2012 IEEE 27th Convention of Electrical and Electronics Engineers in Israel*, IEEE, Eilat, Israel (2012), pp. 1–5, doi: 10.1109/EEEI.2012.6377007.

[18]G. T. Silva, "An expression for the radiation force exerted by an acoustic beam with arbitrary wavefront," J. Acoust. Soc. Am. **130**(6), 3541–3544 (2011).

[19]Z. Gong and M. Baudoin, "Equivalence between angular spectrum-based and multipole expansion-based formulas of the acoustic radiation force and torque," J. Acoust. Soc. Am. **149**(5), 3469–3482 (2021) doi: 10.1121/10.0005004.

[20]A. Marzo, S. A. Seah, B. W. Drinkwater, D. R. Sahoo, B. Long, and S. Subramanian, "Holographic acoustic elements for manipulation of levitated objects," Nature Communications **6**(1), 8661 (2015) doi: 10.1038/ncomms9661.

[21]P. L. Marston, "Axial radiation force of a bessel beam on a sphere and direction reversal of the force," J. Acoust. Soc. Am. **120**(6), 3518 (2006).

[22]P. L. Marston, "Scattering of a bessel beam by a sphere: Ii. helicoidal case and spherical

shell example," J. Acoust. Soc. Am. **124**(5), 2905–2910 (2008).

[23]L. Zhang and P. L. Marston, "Geometrical interpretation of negative radiation forces of acoustical bessel beams on spheres," Phys. Rev. E **84**(3, 2) (2011) doi: 10.1103/PhysRevE.84.035601.

[24]L. Zhang, "A general theory of arbitrary bessel beam scattering and interactions with a sphere," J. Acoust. Soc. Am. **143**(5), 2796–2800 (2018) doi: 10.1121/1.5036734.

[25]M. A. Ghanem, A. D. Maxwell, Y.-N. Wang, B. W. Cunitz, V. A. Khokhlova, O. A. Sapozhnikov, and M. R. Bailey, "Noninvasive acoustic manipulation of objects in a living body," Proceedings of the National Academy of Sciences **117**(29), 16848–16855 (2020) doi: 10.1073/pnas.2001779117.

[26]V. I. Lebedev and D. N. Laikov, "A quadrature formula for the sphere of the 131st algebraic order of accuracy," Doklady Mathematics **59**, 477–481 (1999).

[27]S. L. Sobolev, "Cubature Formulas on the Sphere Invariant under Finite Groups of Rotations," in *Selected Works of S.L. Sobolev*, edited by G. V. Demidenko and V. L. Vaskevich (Springer US, Boston, MA, 2006), pp. 461–466, doi: 10.1007/978-0-387-34149-1_21.

[28]L. V. King, "On the acoustic radiation pressure on spheres," Proceedings of the Royal Society of London. Series A - Mathematical and Physical Sciences **147**(861), 212–240 (1934) doi: 10.1098/rspa.1934.0215.

[29]P. M. Morse and H. Feshbach, *Methods of Theoretical Physics*, Vol. 1 (McGraw-Hill, 1953).

[30]I. S. Gradshteyn and I. M. Ryzhik, *Table of Integrals, Series and Products, Chap. 8 (Eq. 8.533.1)*, 7. ed. ed. (Elsevier Acad. Press, Amsterdam, 2009), p. 1171.

[31]M. Abramowitz and I. Stegun, *Handbook of Mathematical Functions with Formulas, Graphs, and Mathematical Tables*, Applied Mathematics Series (U.S. Government Printing Office, 1948).

[32]J. Z. Buchwald and C.-P. YeangZhao, "Kirchhoff's theory for optical diffraction, its predecessor and subsequent development: the resilience of an inconsistent theory," Arch. Hist. Exact Sci. **70**(5), 463–511 (2016) doi: 10.1007/s00407-016-0176-1.

[33]S. Schot, "80 years of sommerfeld's radiation condition," Historia mathematica **19**(4), 385–401 (1992) doi: 10.1016/0315-0860(92)90004-U.